A Practical Numerical Method to Map the Energy Efficiency of Individual Electro-Hydraulic Drives

Damiano Padovani

Guangdong Technion-Israel Institute of Technology, Shantou, Guangdong, China
damiano.padovani@gtiit.edu.cn

Abstract.

Environmental and economic motivations require urgent improvements to the energy efficiency of hydraulics. In response, the ongoing tendency toward the electrification of fluid power is generating many individual, electro-hydraulic drives. Electric motors drive hydraulic pumps that control the motion of hydraulic actuators without using dissipative flow throttling. Energy efficiency is not constant but varies significantly across the operating range of any given drive and between different architectures. These changes are difficult to predict a priori, prevent a fair comparison between alternatives, and pose a challenge to the designer looking for the best arrangement. The solution is mapping the energy efficiency of the drive for all operating conditions to get a complete overview of its performance. This step is typically done by running countless high-fidelity simulations or experimentally testing the drive on a dedicated test-rig capable of adjusting the load applied to the actuator. Clearly, both approaches are not user-friendly and consume a long time. This research paper presents, therefore, a practical method to derive efficiency maps of electro-hydraulic drives. These maps are based on steady-state equations and require a limited number of parameters obtainable from the literature or published catalogs. The entire procedure does not require experiments, is quick to apply, and reveals the drive's performance and physical limitations with good approximation. The example presented in this study of a single-pump system shows that the drive's overall efficiency stays above 60% in a fairly wide region of the operating range.

Keywords. Efficiency map, energy efficiency, electric motor, inverter, pump, electro-hydraulic, actuator, modeling.

1. INTRODUCTION

Linear hydraulic actuators are crucial devices in many industries due to their distinctive characteristics, such as high-force capability and outstanding reliability. They are typically part of well-established, valve-controlled systems characterized by poor energy efficiency due to flow throttling and the absence of energy recovery [1]. Environmental and economic motivations require urgent improvements in this regard. Thus, the ongoing trends toward the electrification of hydraulics are strengthening the use of individual drives, where the

actuators are coupled to dedicated pumps. These drives can be displacement- or speed-controlled depending on the pump's control element (*i.e.*, its displacement setting or speed, respectively). Concerning the latter variant, multiple arrangements were already proposed involving, for instance, a single pump [2-3], two pumps [4-7], or even three units [8]. The resulting throttleless actuation enhances energy efficiency and enables energy recovery. These electro-hydraulic systems can easily replace conventional valve control in terms of dynamic response [9-10] and energy efficiency [11-12]. However, the energy efficiency is not constant across the drive's working range and varies based on the system architecture and component selection. These changes are difficult to predict a priori and prevent a fair comparison between alternatives. Therefore, a complete map of the system's energy efficiency is an essential tool (it is a chart similar to the ones commonly used for internal combustion engines or electric motors). It gives a good overview of the drive's performance and represents a helpful tool for sizing components. The required approach to obtain such a map is identifying the drive's energy efficiency for all operating conditions. This step is typically done by running countless high-fidelity simulations or experimentally testing the drive on a special test-rig capable of adjusting the external load applied to the actuator [13]. A much faster alternative approach derives the efficiency maps using steady-state mathematical models requiring a limited number of parameters obtainable from the literature or published catalogs. This idea was applied with special emphasis on components, namely a double-rod hydraulic cylinder [14] and a hydrostatic transmission [15], but not on the entire hydraulic system. A more comprehensive perspective was given when mapping the efficiency of a valve-controlled, load-sensing actuator [16], even if it does not involve any electric components. Furthermore, a 1-quadrant efficiency map of a variable-speed, variable-displacement power supply was recently developed [17], but the electric components were modeled with a simplified approach. Schmidt and Hansen derived some 1-quadrant efficiency maps with stress on the electric motor and pump [18]. Their focus was, however, on a study about the potentials of electro-hydraulic drives installed in networks so that the development of those maps was partially addressed.

Consequently, this research paper introduces a practical method to quickly derive efficiency maps, marked by reasonable approximation, of individual electro-hydraulic drives. The focus is on the piston extension against resistant loads, representing the most important working condition. The goal is to establish a generally applicable framework that can easily adjust to any electro-hydraulic drive. Such a comprehensive procedure was not traced in the technical literature despite the increasing popularity of this technology. Closing this gap is, therefore, crucial to fully understanding the system's performance under all operating states and supporting the sizing and selection of the components.

2. SYSTEM MODELING

The electro-hydraulic drive considered in this research is a single-pump system in closed-circuit configuration that requires a minimum number of components. Its layout, shown in Fig. 2.1, depicts the electric motor (EM) that drives the fixed-displacement hydraulic pump (P) used to control the motion of the single-rod hydraulic cylinder (C). The speed of the motor is adjusted by an inverter (I) connected to a DC supply. It can be a common DC-bus when multiple drives are used, or a rectifier if a unique drive is needed. Two pilot-operated check

valves (CVs) compensate for the differential flow of the cylinder. They are connected to a low-pressure line constituted, in this case, by a hydro-pneumatic accumulator (A). It represents a sealed reservoir so that the drive is self-contained (it only requires a wired connection to the electric power supply). Pressure-relief valves located on the actuator ports and a low-pressure filter are omitted for simplicity. These electro-hydraulic drives are capable of operating in four quadrants, if necessary, returning energy back to the DC supply when overrunning loads act on the actuator.

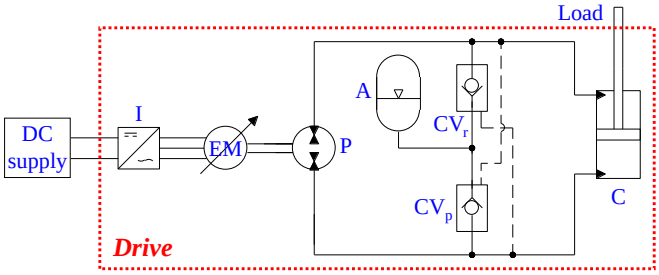

Figure 2.1. Simplified schematic of the individual electro-hydraulic drive chosen as the study case.

Before illustrating the drive's mathematical model, it is worth mentioning the power flows within the system and the different efficiencies. Fig. 2.2 addresses the standard functioning (the power flows from the DC supply to the load).

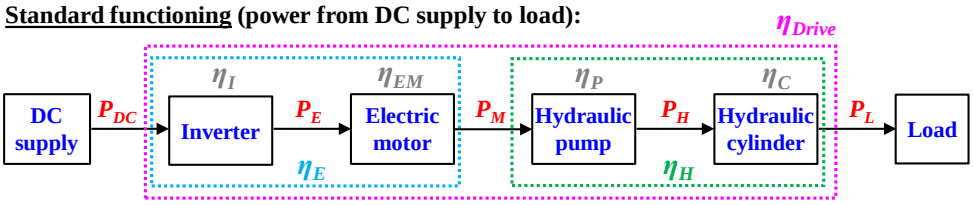

Figure 2.2. Block diagrams of the individual drive highlighting the power flow.

The following subsections describe the approach used to model the energy efficiency of the drive's components.

2.1. Hydraulic actuator

The steady-state force balance of the actuator recalls the hydraulic force (F_H), load force (F_L), and friction force (F_F)

$$F_H = F_L + F_F. \qquad (1)$$

The term F_H depends on the chamber pressures (p_p and p_r) acting on the respective areas (A_p and A_r), whereas the rod-side pressure is set by the low-pressure accumulator. The expression of F_F contains the coefficient of viscous friction (b), the actuator velocity (v), the Coulomb force (F_C), and a constant value (k_1) used to modulate the hyperbolic tangent:

$$F_H = p_p \cdot A_p - p_r \cdot A_r, \quad (2)$$

$$F_F = b \cdot v + \tanh(k_1 \cdot v) \cdot F_C. \quad (3)$$

The piston velocity is obtained by applying the flow conservation to the piston-side of the drive:

$$v = \left(Q_{P,e} - Q_{C,L}\right) \cdot \frac{1}{A_p}, \quad (4)$$

where the effective flow rate of the pump ($Q_{P,e}$) will be elucidated in the next subsection. The same principle enforced to the actuator's rod-side gives the flow through CV_r that is not needed for the purpose of mapping the efficiency. The actuator's mechanical power (P_L), namely the power delivered to the external load, is:

$$P_L = F_L \cdot v. \quad (5)$$

The hydraulic power (P_H) exchanged between the pump and the actuator is defined using the pump's effective flow rate together with the pressure drop (Δp) across the unit:

$$P_H = Q_{P,e} \cdot \Delta p = Q_{P,e} \cdot \left(p_p - p_r\right). \quad (6)$$

The flow leakages across the piston ($Q_{C,L}$) are a function of the pressure drop and a dedicated coefficient (k_L):

$$Q_{C,L} = k_L \cdot \Delta p \ = k_L \cdot \left(p_p - p_r\right). \quad (7)$$

The overall efficiency of the actuator (η_C) is given as:

$$\eta_C = \frac{P_L}{P_H} \cdot 100\%. \quad (8)$$

2.2. Hydraulic pump

The literature lists several analytical models to account for the losses of hydraulic pumps. The chosen approach is a physical-based, steady-state model built on the work of Olsson [19]. It defines the internal flow losses ($Q_{P,L}$) using the four terms in (9) that recall the dissipations due to laminar flow, turbulent flow, fluid compressibility, and constant leakages (Q_K), respectively:

$$Q_{P,L} = \frac{C_L \cdot D \ \cdot \Delta p}{2 \cdot \pi \cdot \mu} + C_T \cdot D^{\frac{2}{3}} \cdot \sqrt{\frac{2 \ \cdot \Delta p}{\rho}} + \frac{D \cdot n \ \cdot \Delta p}{\beta} + \ Q_K. \quad (9)$$

The parameters are the laminar coefficient (C_L), the displacement (D) of the hydraulic unit, the fluid's dynamic viscosity (μ), the turbulent coefficient (C_T), the fluid density (ρ_f), the shaft speed (n), and the fluid's bulk modulus (β).

Similarly, the torque losses ($T_{P,L}$) also include four terms:

$$T_{P,L} = \frac{C_F \cdot D \ \cdot \Delta p}{2 \cdot \pi} + C_D \cdot \mu \ \cdot D \cdot n + \frac{C_H \cdot \rho_f \cdot D^{\frac{5}{3}} \cdot n^2}{4 \cdot \pi} + \ T_K. \quad (10)$$

The latter equation utilizes the coefficients for dry friction (C_F), viscous friction (C_D), hydrodynamic losses (C_H), and constant losses (T_K). These losses are combined with the theoretical quantities ($T_{P,th}$ and $Q_{P,th}$) to calculate the pump's effective flow rate ($Q_{P,e}$) and its effective torque ($T_{P,e}$):

$$Q_{P,th} = D \cdot n\,, \tag{11}$$

$$T_{P,th} = \frac{D \cdot \Delta p}{2 \cdot \pi} = \frac{D \cdot \left(p_p - p_r\right)}{2 \cdot \pi}, \tag{12}$$

$$Q_{P,e} = Q_{P,th} - Q_{P,L} = D \cdot n - Q_{P,L}, \tag{13}$$

$$T_{P,e} = T_{P,th} + T_{P,L} = \frac{D \cdot \Delta p}{2 \cdot \pi} + T_{P,L}. \tag{14}$$

Due to numerical reasons (*e.g*, the model fitting used to estimate the pump losses), a lower saturation sets to zero those negative values, if any, of F_L, v, $Q_{P,e}$, and $T_{P,e}$ so that the sign convention for the first quadrant is enforced.

Thus, both the theoretical and effective mechanical power of the unit (P_M) are derived:

$$P_{M,i} = T_{P,i} \cdot n\,, \qquad i = th, e. \tag{15}$$

Moreover, the efficiencies of the pump also become available, namely the volumetric ($\eta_{P,v}$), mechanical-hydraulic ($\eta_{P,mh}$), and overall ($\eta_{P,t}$) ones:

$$\eta_{P,v} = \frac{Q_{P,e}}{Q_{P,th}} \cdot 100\%, \tag{16}$$

$$\eta_{P,mh} = \frac{T_{P,th}}{T_{P,e}} \cdot 100\%, \tag{17}$$

$$\eta_{P,t} = \frac{P_H}{P_{M,e}} \cdot 100\% \; = \eta_{P,v} \cdot \eta_{P,mh}. \tag{18}$$

2.3. Electric motor

The procedure chosen here for the electric motor leads to an accurate model that requires parameters derived from datasheets (*e.g.*, the one of a PMSM [20]). The power dissipations in the electric machine ($P_{EM,L}$) are originated by three contributions accounting for the copper losses (the stray losses are neglected), iron losses (only in the core), and windage losses [21]:

$$P_{EM,L} = P_{Cu} + P_{Fe} + P_{Wi}, \tag{19}$$

$$P_{Cu} = \frac{1}{2} \cdot q \cdot R_{EM} \cdot \left(\frac{T_{P,th}}{K_T}\right)^2, \tag{20}$$

$$P_{Fe} = \left[K_h \cdot B^2 \cdot f + K_c \cdot B^2 \cdot f^2\right] \cdot m, \tag{21}$$

$$P_{Wi} = (k_2 \cdot n^2 - k_3 \cdot n + k_4) \cdot \pi \cdot \rho_a \cdot n^3 \cdot R_r^4 \cdot L_r. \tag{22}$$

These equations involve the number of phases (q), the winding resistance (R_{EM}), the torque constant (K_T), the coefficient of hysteresis loss (K_h), the frequency ($f = n{\cdot}z/60$) obtained through the shaft speed and the number of poles (z), the coefficient of classical eddy

current's loss (K_c), the peak flux density (B), the core mass of the machine (m), the skin friction coefficient - within brackets in (22) - derived using the constants $k_{2\to4}$, the air density (ρ_a), the rotor radius (R_r), and the rotor length (L_r). The electric power (P_E) and the efficiency of the motor (η_{EM}) result as

$$P_E = P_{M,th} + P_{EM,L}, \tag{23}$$

$$\eta_{EM} = \frac{P_{M,th}}{P_E} \cdot 100\%. \tag{24}$$

It should be noted the theoretical torque is involved. Introducing the effective torque in (20) as well as the effective mechanical power in (23) and (24) leads, in fact, to a slightly distorted efficiency map of the electric motor. The effective torque starts with non-zero values due to modeling the losses such as in (10), so the low-torque region is cut off from the efficiency estimation. Thus, a complete mapping of the motor efficiency is achieved by using the theoretical quantities since this step involves the electric motor alone.

2.4. Inverter

Physic-based modeling of the inverter is possible [22], but this method requires in-depth knowledge of elements, such as transistors, that are not always easily accessible. A simpler technique [23] helps those designers with core expertise in hydraulics. This modeling procedure does not introduce significant differences when compared to more complex approaches since inverters show very high efficiency in almost the entire working range [22].

The inverter's lost power ($P_{I,L}$) is a function of the EM's speed and theoretical torque. Its definition recalls three constant coefficients (c_i):

$$P_{I,L} = c_1 \cdot T_{P,th} + c_2 \cdot T_{P,th}^2 + c_3 \cdot \sqrt{P_{M,th}}\,. \tag{25}$$

The inverter's energy efficiency (η_I) is equal to

$$\eta_I = max\left\{\eta_{I,Min}, \frac{P_{M,th}}{P_{M,th} + P_{I,L}} \cdot 100\%\right\}, \tag{26}$$

where a lower saturation arbitrarily assigns the minimum value ($\eta_{I,Min}$). Again, the theoretical mechanical power of the motor is used for the abovementioned reasons about the map distortion. It is now possible to define the electric power (P_{DC}) drawn from the DC supply that enters the inverter as:

$$P_{DC} = \frac{P_{M,e}}{\eta_I \cdot \eta_{EM}} \cdot 100\%, \tag{27}$$

therefore, using the effective mechanical power of the electric motor, which is dictated by the pump's effective torque, combined with the proper maps of η_I and η_{EM}.

2.5. Drive

After discussing the different components separately, the combination of those partial results leads to the complete analysis of the drive. Its overall efficiency (η_D) includes all the power dissipations taking place in the system:

$$\eta_D = \frac{P_L}{P_{DC}} \cdot 100\% \ = \eta_E \cdot \eta_H = \eta_I \cdot \eta_{EM} \cdot \eta_{P,t} \cdot \eta_{C.} \quad (28)$$

Moreover, the performance of both the electric and hydraulic domains can be addressed distinctly by the electric efficiency (η_E) and the hydraulic efficiency (η_H):

$$\eta_H = \frac{P_L}{P_{M,e}} \cdot 100\% \ = \eta_{P,t} \cdot \eta_C, \quad (29)$$

$$\eta_E = \frac{P_{M,e}}{P_{DC}} \cdot 100\% \ = \eta_I \cdot \eta_{EM}. \quad (30)$$

3. DRIVE'S EFFICIENCY MAPS

The equations given in Section 2 are used to generate the numerical results presented in the sequel. Precisely, (1)-(19) and (23)-(30) constitute a set of 28 independent equations because (15) is repeated twice for the theoretical and effective magnitudes. They are characterized by 31 unknowns (F_F, F_H, F_L, n, P_{DC}, P_E, $P_{EM,L}$, P_H, $P_{I,L}$, P_L, $P_{M,e}$, $P_{M,th}$, p_p, p_r, $Q_{C,L}$, $Q_{P,e}$, $Q_{P,L}$, $Q_{P,th}$, $T_{P,e}$, $T_{P,L}$, $T_{P,th}$, v, η_C, η_D, η_E, η_{EM}, η_H, η_I, $\eta_{P,mh}$, $\eta_{P,t}$, $\eta_{P,v}$). Assigning numerical values to p_p, p_r, and n gives the numerical solution for the remaining 28 unknowns.

The individual drive discussed in [24] is taken as the study case, neglecting the load-holding valves. It controls a single-boom crane that dictates the load-carrying pressure on the piston-side chamber. The highest admitted pressure is 200 bar, the low-pressure side is characterized by $p_r \approx 0$ bar, and the maximum motor speed is assumed to be equal to 3800 rev/min. The vectors of p_p, p_r, and n are assigned using a fixed step for a total of 400 values. Finally, Table I in Appendix A lists all the other parameters required to simulate the system behavior.

3.1. Standard efficiency maps

The drive's overall efficiency is presented in Fig. 3.1 (all the values of the efficiencies are given as percentages). The envelope dictated by the S1 duty curve of the electric motor is also proposed to show the theoretical limit of the operating range (*i.e.*, working points would be

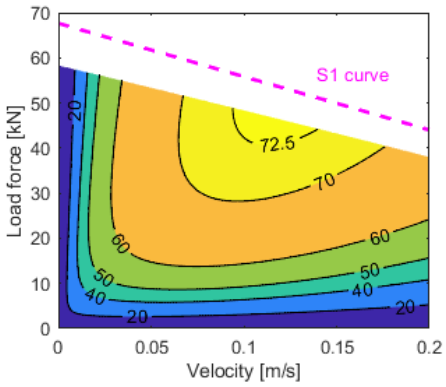

Figure 3.2. Drive's overall efficiency η_D (from DC supply to actuator load).

feasible up to this limit if the system were free of power dissipations). The efficiency's peak value of 73.4% takes place for medium velocity and high force of the actuator. Quantities above 60% are commonplace in a vast portion of the operating range, while poorer behavior is true for very-low piston velocities (<0.03 m/s) and low actuation forces (<15 kN). The global trend in Fig. 3.1 is comparable to the measured one for a similar single-pump system, even if the rectifier is included in that map [25]. It is then worth mentioning that such a performance is aligned with the one of electro-mechanical actuators [25]. In other words, electro-hydraulic drives represent a valid alternative that is also strengthened by other advantages, mainly the higher power output and the faster actuation capabilities [26].

Another asset of the proposed mapping procedure is the opportunity to address the effects of the different components on the drive's overall efficiency. The initial analysis can, for instance, focus on the two domains of the system, namely the electric and the hydraulic ones (Fig. 3.2). These charts show that the electric components have a global efficiency above 85% for a large range. The hydraulic elements, on the contrary, ensure a good combined efficiency above 75% only when the force delivered by the actuator is significant (at least one-third of the maximum). It should be noted that the top value of the hydraulic efficiency is approximately 80%; it refers to the conversion between the mechanical power of the pump's shaft and the one of the load. Such a result is encouraging when compared to valve-controlled systems; for instance, the hydraulic efficiency of a single, load-sensing actuator deteriorates faster when leaving the sweet spot [16].

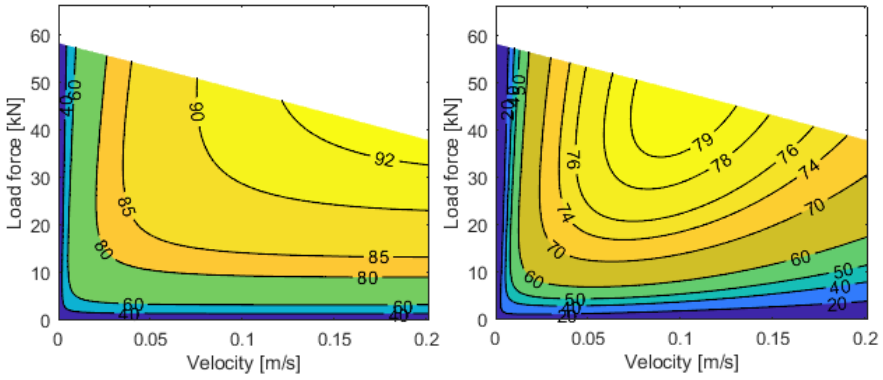

Figure 3.2. Drive's electric efficiency η_E on the left (from DC supply to electric motor's shaft) and hydraulic efficiency η_H (from motor's shaft to load).

Moving a step further, emphasis is placed on the efficiency of all components. Starting from the inverter (Fig. 3.3), its efficiency is well above 94%, with the only exception of the EM's low-speed operations. This behavior is true for popular Si-IGBT inverters, but improvements in that critical area are possible when selecting GaN-MOSFET inverters [22].

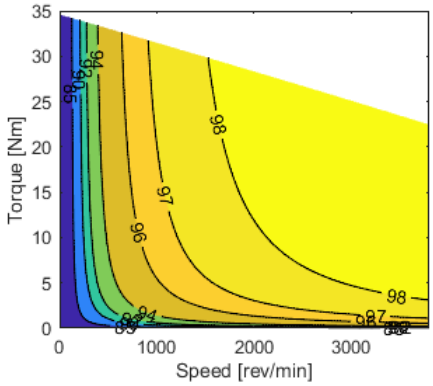

Figure 3.3. Inverter efficiency η_I (from DC supply to inverter outlet).

Then, the electric motor has a limited impact on the drive performance. Its efficiency remains sufficiently high, above 80%, on almost the entire range (Fig. 3.4). Those numbers can easily improve when the machine's rated power increases since it is well-known that powerful electric motors have higher efficiencies. Fig. 3.4 also reports the S1 duty curve of the PMSM. The upper limit of the speed in the plot (3800 rev/min) is the one leading to the maximum power output. For higher angular velocities up to the maximum admitted one (4200 rev/min), the outputted power drops down dramatically so that this portion of the operating range is ignored.

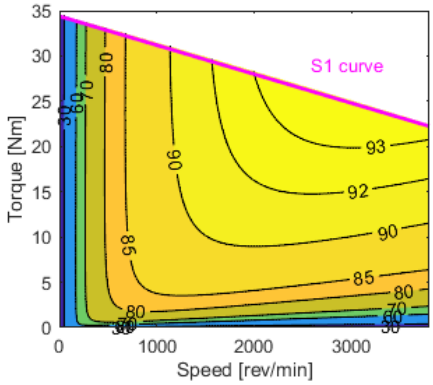

Figure 3.4. Electric motor's efficiency η_{EM} (from inverter outlet to motor shaft).

Moving to the hydraulic domain, the pump has a major impact on the drive performance (Fig. 3.5). Even if the pump's overall efficiency results are acceptable (it is greater than 60% almost everywhere for standard operations), its maximum value of 81.9% is limited. Such a behavior is representative of an axial-piston machine that does not employ the most recent findings being published to enhance efficiency and whose loss coefficients in (9) and (10) were tuned

to mimic the loss maps reported in [27]. Hydraulic units with newer designs will improve these numbers, as will machines with bigger displacements.

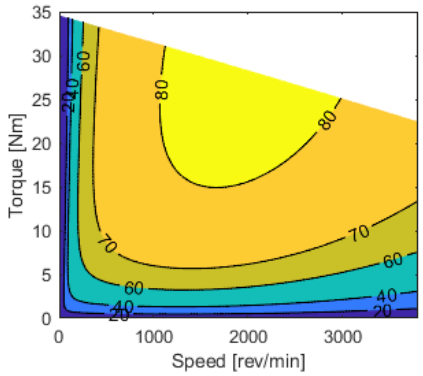

Figure 3.5. Pump's overall efficiency $\eta_{P,t}$ (from motor's shaft to pump outlet).

Finally, the influence of the hydraulic cylinder is minimal (Fig. 3.6). Its efficiency exceeds 90% in a wide range and stays above 95% for typical operations characterized by average velocities and medium-to-high forces.

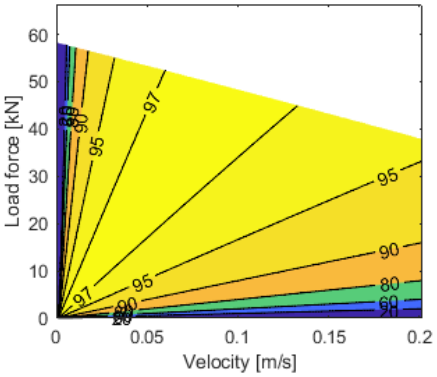

Figure 3.6. Actuator's efficiency η_C (from pump outlet to load).

3.2. Dimensionless efficiency maps

The possibility of plotting nondimensional magnitudes enables the most general understanding of the system behavior. The chart in Fig. 3.7, which depicts the drive's overall efficiency, was derived by dividing the magnitudes in the x and y directions with their maximum values (66.4 kN and 0.2 m/s). Reconstructing dimensional quantities via the inverse process can address similar drives of other sizes. This step offers an approximated estimation of the system performance without performing any simulations. However, this process will underestimate the efficiency of more powerful drives than the one used to derive the previous graphs (*i.e.*, installed power of 8.8 kW) for the already mentioned reasons about

the efficiency improvements as the size of the components grows. Lastly, the same approach can also be applied to the other maps in Fig. 3.2-Fig. 3.6, but it is omitted for brevity.

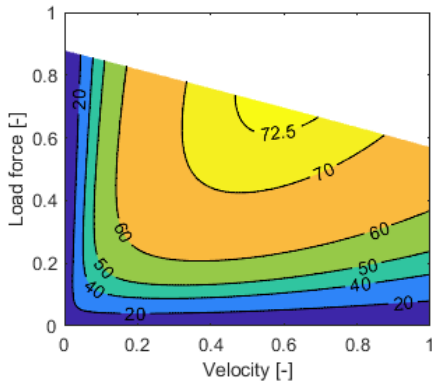

Figure 3.7. Dimensionless map of the drive's overall efficiency η_D (from DC supply to actuator load).

4. APPLICATIONS OF THE DRIVE'S EFFICIENCY MAP

4.1. Identifying the power limits

The efficiency maps derived before can also show the power managed by the drive. Useful insight is derived on the achievable power output and on the required power input. The plots in Fig. 4.1 clearly highlight the system limitations and are extremely valuable in predicting the suitability of the drive to perform a given task.

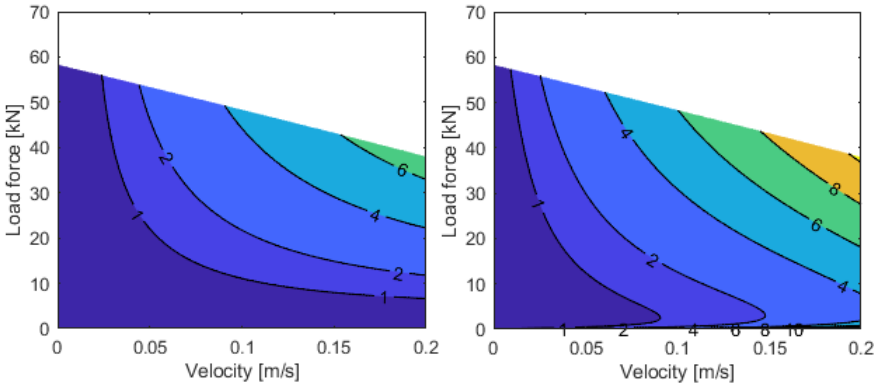

Figure 4.1. Power managed by the drive: mechanical power ouput P_L (left) and electric power input P_{DC} (right) in kW.

For the compact system assumed as the study case, the maximum outputted power is 6.9 kW, while the average values are within 3-5 kW for medium-to-high actuation velocities

and forces. Conversely, the electric power taken from the DC supply can increase up to 10.3 kW, even if it is often close to 4-7 kW during representative operations.

4.2. Supporting the component selection

This subsection shows another powerful application of the proposed method by considering an alternative component. Due to the impact of the pump on the overall performance, the effects of a more efficient hydraulic unit are predicted. For simplicity, the power losses of the original unit are reduced by 50% in any operating condition to arbitrarily consider feasible improvements. The new overall efficiency map of the pump in Fig. 4.2 displays that the peak efficiency increases up to 90.4%, as opposed to 81.9% of the initial set-up (Fig. 3.5). Most importantly, the efficiency is now above 70% almost everywhere, at least for standard operations (exceptions take place at very low torques and speeds).

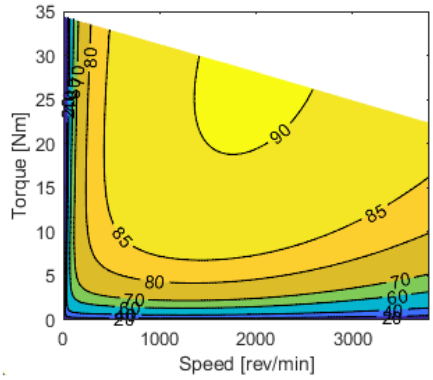

Figure 4.2. Hydraulic pump's overall efficiency $\eta_{P,t}$ for the alternative set-up.

The resulting improvements in the drive's overall efficiency and hydraulic efficiency emerge from Fig. 4.3.

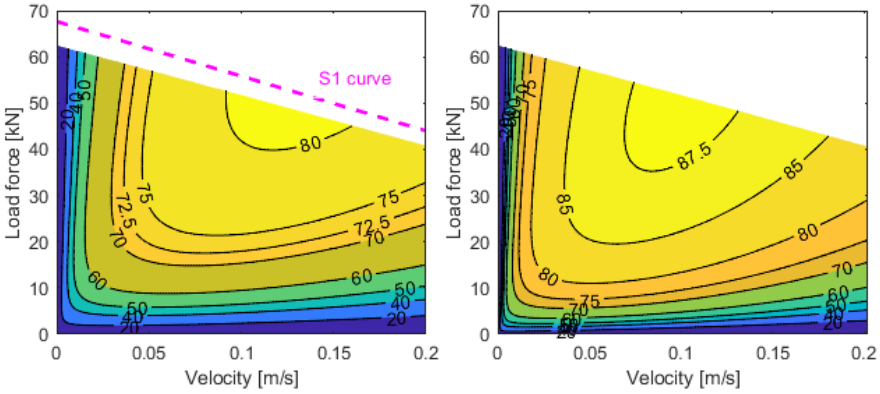

Figure 4.3. Drive's overall efficiency η_D (left) and drive's hydraulic efficiency η_H (right) for the alternative set-up.

First, the working area is expanded toward higher power levels (its upper margin is getting closer to the theoretical limit of the S1 curve). Values of at least 70% for the overall efficiency are commonplace, with the highest number at 80.8% as opposed to 73.4% for the original case. A similar benefit concerns the hydraulic efficiency that results superior to 80% in a wide range. However, it is worth noticing that both efficiencies do not improve greatly for unconventional operations characterized by very low actuation velocities (below 0.03 m/s) and medium-to-low actuation forces (under 15 kN, namely about one-fourth of the maximum transmissible force).

5. CONCLUSIONS

The ongoing trend toward the electrification of hydraulics requires user-friendly tools to further develop electro-hydraulic drives. This research paper contributes to increasing the understanding of those systems as follows:

- A generally applicable method is introduced to quickly derive efficiency maps for electro-hydraulic systems. This approach is defined as numerical because it is based on steady-state equations that use a limited number of parameters obtainable from the literature, or from catalogs (*i.e.*, experiments are not involved).
- It is possible to explore the behavior of the drive for all operating conditions and support the process of sizing and selecting the components. Efficiency maps of the single components are also obtained.
- The example of a single-pump drive confirmed that this throttleless technology is very promising. The peak efficiency of 73.4% was calculated when converting the electric power entering the inverter into the mechanical power leaving the actuator. It was also shown that the pump has the biggest influence on the overall efficiency, highlighting, therefore, a direction for future improvements.

In short, this generally applicable framework, which is adjustable to any electro-hydraulic drive, helps us better understand those energy-efficient solutions.

APPENDIX A

TABLE I. VALUES OF THE DRIVE'S PARAMETERS

A_p	3318.30	mm^2	K_c	$76.59/10^7$	$W/Hz/T^2/kg$
A_r	2356.20	mm^2	K_h	$56.26/10^3$	$W/Hz/T^2/kg$
b	8000.00	kg/s	k_L	$0.25/10^{12}$	$m^3/s/Pa$
B	1.30	T	K_T	2.05	Nm/A
c_1	2.00	kW/(Nm)	L_r	0.25	m
c_2	$5.00/10^4$	$kW/(Nm)^2$	m	16.20	kg
c_3	0.50	$kW/(Nm \cdot rad/s)^{1/2}$	q	3.00	-
C_D	$-11.32 \cdot 10^4$	-	Q_K	$15.39/10^2$	L/min

C_F	$56.46/10^3$	-
C_H	985.50	-
C_L	$57.94/10^5$	-
C_T	$95.07/10^6$	-
D	10.60	cm^3/rev
F_C	75.00	N
k_1	$5.00/10^3$	-
k_2	$87.07/10^{11}$	min^2/rev^2
k_3	$60.69/10^7$	min/rev
k_4	$19.18/10^3$	-

R_{EM}	0.79	Ω
R_r	$7.50/10^2$	m
T_K	20.34/10	Nm
z	4.00	-
β	3329.00	bar
$\eta_{I,Min}$	80	%
μ	$3.93/10^2$	Ns/m^2
ρ_a	10.09/10	kg/m^3
ρ_f	855.00	kg/m^3

6. REFERENCES

[1] D. Padovani, M. Rundo, and G. Altare, "The Working Hydraulics of Valve-Controlled Mobile Machines: Classification and Review," *ASME J. Dyn. Syst. Meas. Control*, vol. 142, no. 7, 2020.

[2] S. Michel and J. Weber, "Energy-efficient electrohydraulic compact drives for low power applications," *ASME/BATH Symp. Fluid Power Motion Control*, 2012.

[3] D. Padovani, S. Ketelsen, and L. Schmidt, "Downsizing the Electric Motors of Energy-Efficient Self-Contained Electro-Hydraulic Systems by Using Hybrid Technologies," *BATH/ASME Symp. Fluid Power Motion Control*, 2020.

[4] T. Minav, M. P. J.E. Heikkinenb, J. E. Heikkinen, and M. Pietola, "Direct driven hydraulic drive for new powertrain topologies for non-road mobile machinery," *Electr. Power Syst. Res.*, vol. 152, Nov. 2017.

[5] L. Schmidt, S. Ketelsen, D. Padovani, and K. Mortensen, "Improving the Efficiency and Dynamic Properties of a Flow Control Unit in a Self-Locking Compact Electro-Hydraulic Cylinder Drive," *ASME/BATH Symp. Fluid Power Motion Control*, 2019.

[6] G. Kolks and J. Weber, "Electro-Hydrostatic Compact Drives with Variable Transmission Ratio," *12th Int. Fluid Power Conf.*, 2020.

[7] S. Ketelsen, D. Padovani, M. K. Ebbesen, T. O. Andersen, and L. Schmidt, "A Gasless Reservoir Solution for Electro-Hydraulic Compact Drives with Two Prime Movers," *ASME/BATH Symp. Fluid Power Motion Control*, 2020.

[8] L. Schmidt, M. Groenkjaer, H. C. Pedersen, and T. O. Andersen, "Position Control of an Over-Actuated Direct Hydraulic Cylinder Drive," *Control Eng. Pract.*, vol. 64, 2017.

[9] D. Hagen, D. Padovani, and M. Choux, "A Comparison Study of a Novel Self-Contained Electro-Hydraulic Cylinder versus a Conventional Valve-Controlled Actuator — Part 1 : Motion Control," *Actuators*, vol. 8, no. 79, 2019.

[10] D. Padovani, "Adding Active Damping to Energy-Efficient Electro-Hydraulic Systems for Robotic Manipulators — Comparing Pressure and Acceleration Feedback," *IEEE 5th Int. Conf. on Robotics and Automation Engineering*, 2020.

[11] D. Hagen, D. Padovani, and M. Choux, "A Comparison Study of a Novel Self-Contained Electro-Hydraulic Cylinder versus a Conventional Valve-Controlled

Actuator — Part 2: Energy Efficiency," *Actuators*, vol. 8, no. 78, 2019.
[12] S. Qu, D. Fassbender, A. Vacca, and E. Busquets, "A High-Efficient Solution for Electro-Hydraulic Actuators with Energy Regeneration Capability," *Energy*, vol. 216, 2021.
[13] S. Qu, D. Fassbender, A. Vacca, and E. Busquets, "A Cost-Effective Electro-Hydraulic Actuator Solution with Open Circuit Architecture," *Int. J. Fluid Power*, vol. 22, no. 2, 2021.
[14] N. Manring, "Efficiency Mapping for a Linear Hydraulic-Actuator," *ASME J. Dyn. Syst. Meas. Control. Tech. Br.*, 2013.
[15] N. Manring, "Mapping the Efficiency for a Hydrostatic Transmission," *ASME J. Dyn. Syst. Meas. Control*, vol. 138, no. 3, 2016.
[16] L. Manring and N. Manring, "Mapping the Efficiency of a Double Acting, Single-Rod Hydraulic-Actuator Using a Critically Centered Four-Way Spool Valve and a Load-Sensing Pump," *ASME J. Dyn. Syst. Meas. Control*, vol. 140, no. 9, 2018.
[17] H. T. Phan and Y. Sato, "Improving the Overall Efficiency of an Electro-hydraulic Drive System by using Efficiency Maps," *JFPS Int. J. Fluid Power Syst.*, vol. 14, no. 1, 2021.
[18] L. Schmidt and K. V. Hansen, "Electro-Hydraulic Variable-Speed Drive Networks—Idea, Perspectives, and Energy Saving Potentials," *Energies*, vol. 15, no. 3, 2022.
[19] O. Olsson, "Matematisk Verkingsgradmodell (Mathematical Efficiency Model)," Institute of Technology, Linköping, Sweden, 1973.
[20] Bosch Rexroth AG, "Rexroth IndraDyn S MSK Synchronous Motors," Lohr a. Main, Germany, 2006.
[21] C. Huynh, L. Zheng, and D. Acharya, "Losses in High Speed Permanent Magnet Machines Used in Microturbine Applications," *ASME J. Eng. Gas Turbines Power*, vol. 131, no. 2, 2009.
[22] K. Kumar, "Efficiency Improvement of Three Phase Traction Inverter through GaN Devices for PMSM," *IEEE Int. Conf. on Power Electronics, Drives and Energy Systems*, 2016.
[23] A. Ritari, J. Vepsäläinen, K. Kivekäs, K. Tammi, and H. Laitinen, "Energy Consumption and Lifecycle Cost Analysis of Electric City Buses with Multispeed Gearboxes," *Energies*, vol. 13, no. 8, 2020.
[24] D. Padovani, S. Ketelsen, D. Hagen, and L. Schmidt, "A self-contained electro-hydraulic cylinder with passive load-holding capability," *Energies*, vol. 12, no. 2, 2019.
[25] S. Michel, "Elektrisch-Hydrostatische Kompaktantriebe mit Differentialzylinder für die Industrielle Anwendung," Technischen Universität Dresden, Germany, 2021.
[26] D. Hagen, D. Padovani, and M. Choux, "Guidelines to Select Between Self-Contained Electro-Hydraulic and Electro-Mechanical Cylinders," *IEEE 15th Conf. on Industrial Electronics and Applications*, 2020.
[27] D. Padovani, "Leveraging Flow Regeneration in Individual Energy-Efficient Hydraulic Drives," *ASME/BATH Symp. Fluid Power Motion Control*, 2021.

Biographies

Damiano Padovani joined the Guangdong Technion-Israel Institute of Technology in 2021. He received his B.Sc. and M.Sc. degrees in Mechanical Engineering from the Polytechnic University of Turin (Italy) and his Ph.D. degree in Engineering with a specialization in Fluid Power from Purdue University (USA). He worked as a post-doc researcher at Vanderbilt University (USA), as a faculty member at the University of Agder (Norway), and in the industry with Parker Hannifin (USA). His research interests focus on different aspects of fluid power, mainly embracing energy efficiency, mobile hydraulics, and applied control.